THE JOURNAL OF BIOLOGICAL CHEMISTRY VOL. 285, NO. 22, pp. 16513–16520, May 28, 2010

Properties of the TRPML3 Channel Pore and Its Stable Expansion by the Varitint-Waddler-causing Mutation*[S]

Received for publication, October 22, 2009, and in revised form, April 7, 2010 Published, JBC Papers in Press, April 8, 2010, DOI 10.1074/jbc.M109.078204

Hyun Jin Kim[‡1], Soichiro Yamaguchi[‡1], Qin Li[‡], Insuk So[§], and Shmuel Muallem[‡2]

From the [‡]Department of Physiology, University of Texas Southwestern Medical Center, Dallas, Texas 75390 and the [§]Department of Physiology and Biophysics, Seoul National University College of Medicine, Seoul 110-799, Korea

TRPML3 is a H^+-regulated Ca^{2+} channel that shuttles between intracellular compartments and the plasma membrane. The A419P mutation causes the varitint-waddler phenotype as a result of gain-of-function (GOF). The mechanism by which A419P leads to GOF is not known. Here, we show that the TRPML3 pore is dynamic when conducting Ca^{2+} to change its conductance and permeability, which appears to be mediated by trapping Ca^{2+} within the pore. The pore properties can be restored by strong depolarization or by conducting Na^+ through the pore. The A419P mutation results in expanded channel pore with altered permeability that limits modulation of the pore by Ca^{2+}. This effect is specific for the A419P mutation and is not reproduced by other GOF mutations, including A419G, H283A, and proline mutations in the fifth transmembrane domain. These findings describe a novel mode of a transient receptor potential channel behavior and suggest that pore expansion by the A419P mutation may contribute to the varitint-waddler phenotype.

TRPML3 belongs to the TRPML subfamily of the transient receptor potential (TRP)[3] channels superfamily (1, 2). The subfamily consists of TRPML1, mutations in which cause the lysosomal storage disease mucolipidosis type IV (3), TRPML2 and TRPML3. The A419P mutation in the putative fifth transmembrane domain (TMD) of TRPML3 causes the varitint-waddler phenotype that is characterized by pigmentation defect, hearing loss, circling behavior, and embryonic lethality (4, 5).

TRPML3 functions as an inwardly rectifying cation channel (6), with high Ca^{2+}/K^+ selectivity (7–10) and shuttles between the plasma membrane and intracellular organelles to regulate membrane trafficking (11, 12) and autophagy (11). Recently, we reported a unique form of regulation of TRPML3 by extracytosolic (luminal) Na^+ and H^+ ($H^+_{e\text{-}cyto}$), which is mediated by a string of three histidines (His^{252}, His^{273}, and His^{283}) in the large extracytosolic loop between TMD1 and TMD2 (7). Binding of H^+ to His^{283} inhibits the channel, whereas His^{252} and His^{273} hinder H^+ access to His^{283}. Interestingly, preventing H^+ binding to His^{283} resulted in a gain-of-function (GOF) that increases Ca^{2+} influx and causes marked cell toxicity (7). Regulation of TRPML3 function by binding of H^+ to His^{283} suggested the possibility that the loop communicates with the pore domain and the communication is regulated by H^+ binding to His^{283}. This possibility is further suggested by elimination of the regulation by $H^+_{e\text{-}cyto}$ by the A419P mutation in the fifth TMD of TRPML3 (7).

We (6) and others (8–10) have shown that the A419P mutation is a GOF mutation that locks TRPML3 in an open conformation. The mechanism by which the A419P mutation leads to GOF is not known. Although elimination of the inhibition of TRPML3 activity by $H^+_{e\text{-}cyto}$ plays a role in the GOF (7), the A419P mutation may also affect the pore selectivity and conductance. Because proline introduces a kink or a break in α-helical transmembrane spans, and the A419G mutation that may disrupt α-helical structures results in a similar GOF in TRPML3 as the A419P (6, 9), it was postulated that the GOF by TRPML3(A419P) is caused by destabilization of the fifth TMD helix of TRPML3 (9, 13). However, it is still unclear how the proline-induced destabilization of the fifth TMD affects the behavior of the TRPML3 pore to lead to the GOF.

Very little is known of the properties of the TRPML3 pore. As indicated above, the pore of the wild-type (WT) channel shows high Ca^{2+}/K^+ and Ca^{2+}/Cs^+ selectivity with similar Na^+ and Ca^{2+} conductance at isotonic ion concentrations (7). With limited exceptions, ionic selectivity and conductance are considered constant and defining features of ion channels. The best known examples of ion channels with variable permeability are the ionotropic P2X receptors, which undergo time-dependent slow pore expansion subsequent to activation with their ligands (14–16). Other recent examples are the TRPV1 and TRPA1 channels. TRPV1 undergoes time-dependent pore expansion following agonist stimulation (17), with the agonist type controlling the rate of pore expansion (17) and Ca^{2+}/Na^+ conductance ratio (18). Ligand stimulation dilates the TRPA1 pore (19, 20) and increases its Ca^{2+}/Na^+ selectivity ratio (19).

To understand better the molecular mechanism of the varitint-waddler phenotype, we characterized the pore properties of WT TRPML3 and several TRPML3 mutants, including TRPML3(A419P). We report that the TRPML3 pore is dynamic and undergoes spontaneous, Ca^{2+}-dependent modulation when conducting Ca^{2+}. The A419P mutation alters this behavior by stably expanding the pore. Interestingly, several GOF mutations, and in particular H283A in the extracytosolic loop

* This work was supported in part by National Institutes of Health Grants DE12309 and DK38938 and the Ruth S. Harrell Professorship in Medical Research.

[S] The on-line version of this article (available at http://www.jbc.org) contains supplemental Figs. S1 and S2 and Tables 1 and 2.

[1] Both authors contributed equally to this work and should be considered first coauthors.

[2] To whom correspondence should be addressed. E-mail: shmuel.muallem@utsouthwestern.edu.

[3] The abbreviations used are: TRP, transient receptor potential; TMD, transmembrane domain; GOF, gain-of-function; WT, wild type; E_{rev}, reversal potential; BAPTA, 1,2-bis(2-aminophenoxy)ethane-*N*,*N*,*N*′,*N*′-tetraacetic acid; NMDG, *N*-methyl-D-gluconate.

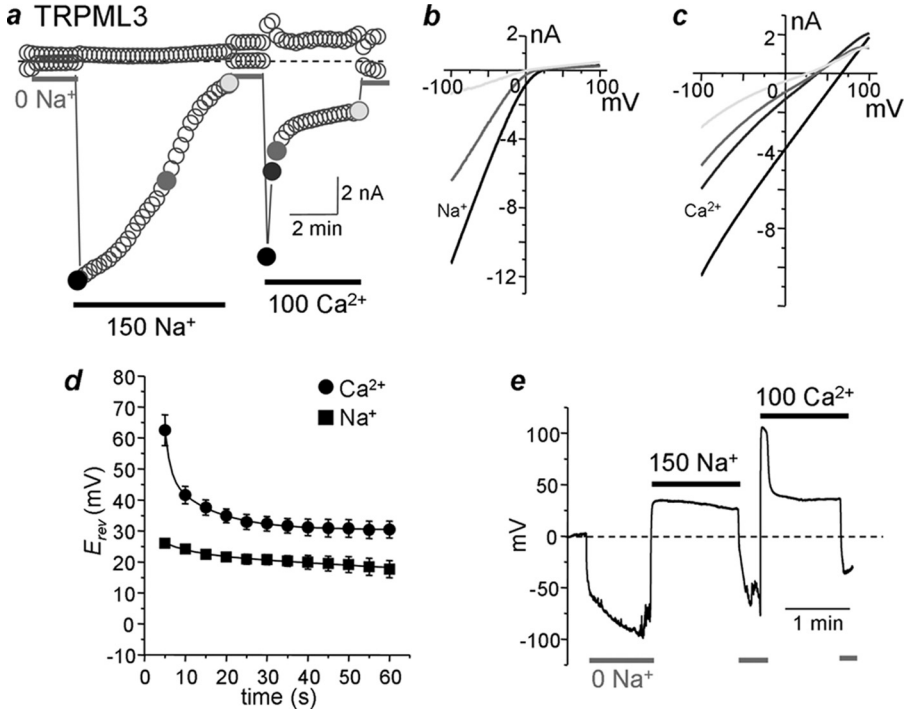

FIGURE 1. **Dynamic behavior of the TRPML3 pore.** *a*, whole cell current was measured in HEK cells transfected with WT TRPML3. The major cation in the pipette solution was 150 mM Cs^+, and Ca^{2+} was buffered close to 0 with 10 mM BAPTA. The major cation in the bath solution was 150 mM Na^+ (*black bars*), 150 mM $NMDG^+$ (*light gray bars*), or 100 mM Ca^{2+} (*black bars*). TRPML3 was activated by exposing the cells to Na^+-free bath solution. After measurement of the maximal Na^+ current, the cells were exposed to 100 mM Ca^{2+}. Shown is the current measured at −100 (*lower circles*) and +100 mV (*upper circles*). *Dashed lines* here and in all other figures indicate the 0 current levels. *b* and *c*, *I/V* relationships of the TRPML3 current recorded at the times shown in the *large black circles* in *a*. *d*, changes in E_{rev} during the first 1 min of WT TRPML3 in 150 Na^+ (*squares*) and 100 Ca^{2+} (*circles*). The results are the mean ± S.E. of seven experiments. *e*, current clamp protocol was used to record the membrane potentials.

and the A419G in the fifth TMD, do not affect pore behavior. These findings describe a unique behavior of the TRPML3 pore and provide a molecular mechanism for the GOF in the varitint-waddler phenotype.

MATERIALS AND METHODS

Plasmid Construction, Mutagenesis, Reagents, and Cells—Full-length human TRPML3 was amplified from human placenta and cloned into the pEGFPC1 and p3XFLAG-CMV-7.1 vectors, as described before (7). The full-length sequence corresponding to the human TRPML1 coding region was amplified by PCR using IMAGE clone BF 529860 as template, and the amplified product was subcloned into pEGFPC1. The QuikChange mutagenesis kit was used to introduce mutations by following the manufacturer's instructions. All mutations were confirmed by sequencing the entire open reading frame to verify the presence of the desired mutation and the absence of extraneous mutations. All reagents were purchased from Sigma. HEK293 cells were maintained in Dulbecco's modified Eagle's medium supplemented with 10% fetal bovine serum. One day after plating, cells were transfected with Lipofectamine 2000 and used for current recording 24 h later.

Current Recordings—The TRPML3 current was recorded at room temperature using the whole-cell configuration of the patch clamp technique. The patch electrodes had a resistance of 3–5 MΩ. Series resistance values were generally below 15 MΩ and were not compensated for. Data were collected and analyzed using an Axopatch 200 amplifier and pClamp 9.2 software. Currents were measured by application of −100 to +100 mV, 100-ms voltage RAMPs every 1 or 5 s from a holding potential of 0 or +80 mV. Unless otherwise indicated, the pipette solution contained 130 mM cesium aspartate, 20 mM CsCl, 1 mM $MgCl_2$, 4 mM Na_2-ATP, 10 mM HEPES, and 10 mM BAPTA. In some experiments, as indicated, 2 mM $CaCl_2$ and 2 mM EGTA were added to the standard pipette solution instead of 10 mM BAPTA to clamp Ca^{2+} at 10 μM. Effectively, this solution has no mobile Ca^{2+} buffer because most of the EGTA is bound with the added Ca^{2+}. The standard bath solution contained 140 mM NaCl, 5 mM KCl, 1 mM $MgCl_2$, 1 mM $CaCl_2$,10 mM glucose, and 10 mM HEPES, adjusted to pH 7.4 with NaOH. The Na^+-free solution contained 150 mM NMDG-Cl, 5 mM EGTA, and 10 mM HEPES, adjusted to pH 7.4. Ca^{2+}-containing solutions were prepared by isosmotically replacing $NMDG^+$ with Ca^{2+} in the Na^+-free solution. Monovalent ion solutions contained 150 mM monovalent ions instead of $NMDG^+$ in the Na^+-free solution, adjusted to pH 7.4 with NMDG-OH.

Orai1 current was recorded with the same pipette solution used to record the TRPML3 current. The channel was activated by passive store depletion with 10 mM BAPTA in the pipette solution, and the current was initiated by perfusing the cells with a solution containing 105 mM $CaCl_2$ and 10 mM HEPES, pH 7.4. Current was measured by −100 to +100 mV, 100-ms RAMPs every 1 s from a holding potential of 0 mV.

Data Analysis—The permeability ratios of monovalent cations relative to Na^+ were calculated from the shift in reversal potential (ΔE_{rev}) on changing the extracellular solutions using the question $P_X/P_{Na} = \exp(\Delta E_{rev} x F/RT)$, where R, T, and F have their usual meaning. The shift in E_{rev} was determined relative to Na^+ in the same cells to nullify any effect of the leak current on E_{rev}. All potentials were corrected for liquid junction potentials using the program JPCalcW (Axon Instruments). χ^2-distribution for two exponential fits of change in E_{rev} time course was about 10 times better than single exponential fits, and thus the changes in E_{rev} are mostly fitted with two exponentials. Pore diameter was estimated by fitting the currents to the modified excluded volume equation: $P_X/P_{Na} = (dP - dX/dP - dNa)^2$, where dP, dX, and dNa are diameters of the pore, cation X^+, and Na^+, respectively. Data are shown as mean ± S.E. of the indicated number of observations.

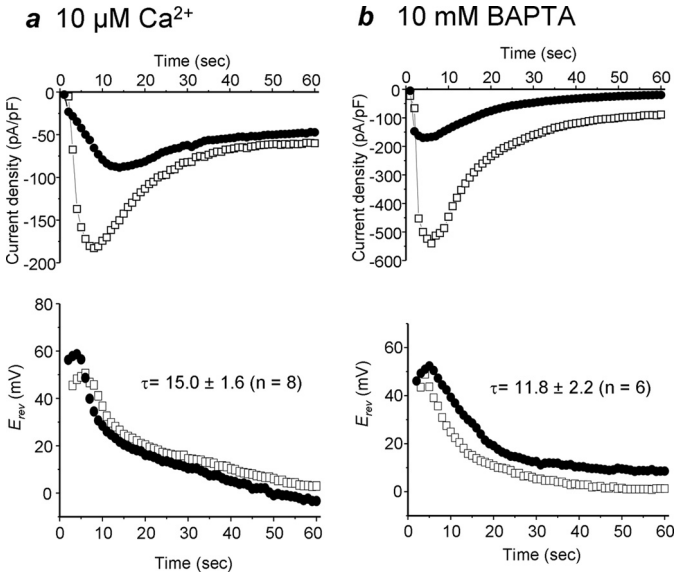

FIGURE 2. **Effect of the Ca^{2+} buffer and current density on E_{rev}.** Cells expressing TRPML3 were dialyzed with pipette solutions containing either 10 μM Ca^{2+} (2 mM EGTA + 2 mM $CaCl_2$) (*a*) or 10 mM BAPTA (*b*). The current was recorded every second by the RAMPs protocol described under "Materials and Methods." The figure shows example traces with two different current densities. The average time constants obtained from single exponential fits are given as mean ± S.E. of the indicated number of experiments.

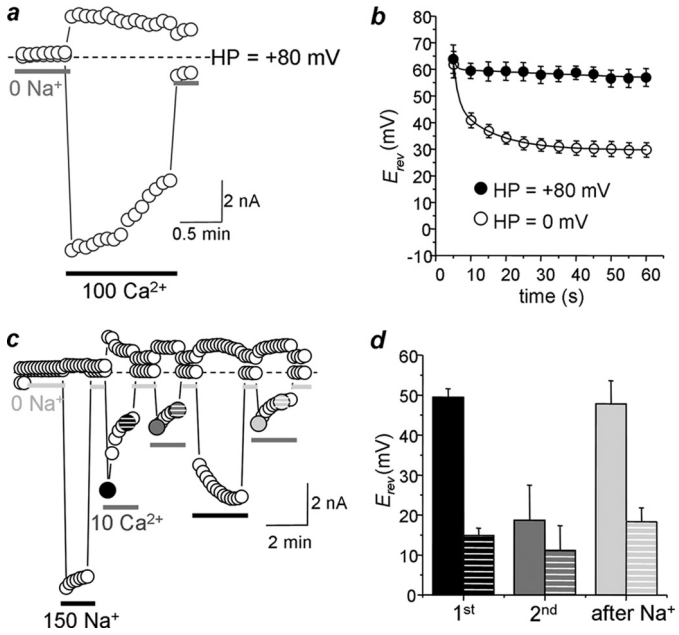

FIGURE 3. **Modulation of TRPML3 activity by Ca.** *a*, Ca^{2+} current of WT TRPML3 was measured as in Fig. 1*a*, except that the holding potential (*HP*) was +80 mV. *b*, E_{rev} changes during the first 1 min of current recording for WT TRPML3 in 100 Ca^{2+} solutions at holding potentials of +80 mV (*filled circles*) and 0 mV (*open circles*). The latter is reproduced from Fig. 1*d* to facilitate comparison. The results at +80 mV are the mean ± S.E. of three experiments. *c*, Na^+ and Ca^{2+} currents of WT TRPML3 were measured as in Fig. 1, except that at the periods marked by *gray bars* the cells were incubated in 10 mM Ca^{2+}-containing Na^+-free bath solution. All Na^+-free solutions contained 5 mM EGTA. Note that after conducting Ca^{2+}, both Na^+ and Ca^{2+} currents are strongly inhibited. *d*, mean ± S.E. (*error bars*) of the E_{rev} recorded at the times shown in the *large filled circles* in *c* in 10 mM Ca^{2+} during the first and second exposure to Ca^{2+} and the recovery after relief of the inhibition by conduction of Na^+ by the channel ($n = 4$). The first columns are the initial E_{rev}, and the *striped columns* are the E_{rev} after 30-s exposure to 10 mM Ca^{2+}.

RESULTS AND DISCUSSION

Behavior of the TRPML3 Pore—In a previous study, we reported that WT TRPML3 is a selective Ca^{2+} channel (6). The current was recorded by −100 to +100 mV voltage RAMPs from a holding potential of 0 mV every 5 s. As was shown previously (6, 7), short incubation of cells expressing WT TRPML3 in Na^+-free solution and readdition of Na^+ resulted in a large strongly inward rectifying current that slowly inactivates in the continuous presence of Na^+_o (Fig. 1*a*). Incubation in isosmotic Ca^{2+} following the exposure to Na^+-free medium evoked a large inward current that undergoes partial fast inactivation and stabilization at a plateau of about 25% of the initial current (Fig. 1*a*). The current/voltage (I/V) relationship of the Na^+ current (Fig. 1*b*) showed only a slight shift in E_{rev}, even 5 min after channel opening. By contrast, the Ca^{2+} current displays a large shift in E_{rev} during the first two to three sweeps (Fig. 1*c*). The analysis in Fig. 1*d* and supplemental Table 1 show that the shift in E_{rev} of the Ca^{2+} current could be fitted well with two exponentials. E_{rev} was also recorded using current clamp (Fig. 1*e*). The hyperpolarization observed on exposure to Na^+-free medium reflects the rate of channel activation in the absence of external permeable cations. Incubation in isotonic Na^+ resulted in a small stable depolarization. On the other hand, incubation in isosmotic Ca^{2+} resulted in a large but transient depolarization, similar to the shift in E_{rev} in Fig. 1*d*. However, notably, the decay in E_{rev} of the Ca^{2+} current in Fig. 1*e* was fitted best to a single exponential.

Although cytoplasmic Ca^{2+} accumulation likely accounts for part of the shift in E_{rev}, most of the shift may be caused by a change in channel pore properties. An attempt to increase the Ca^{2+} buffer by increasing pipette BAPTA to 30 and 50 mM, to reduce the effect of accumulated Ca^{2+} on E_{rev}, was not feasible because this resulted in inactivation (50 mM) or altered properties (30 mM) of the channel. Therefore, to determine whether a change in channel Ca^{2+} selectivity contributes to the shift, we determined whether the E_{rev} shift is influenced by current density and the cytoplasmic mobile Ca^{2+} buffer. In Fig. 2 we compared the shift in E_{rev} in cells dialyzed with pipette solution containing 10 μM Ca^{2+} buffered with 2 mM EGTA (no free buffer) and pipette solution containing 10 mM BAPTA and at two current densities. External Ca^{2+} was reduced to 10 mM to reduce Ca^{2+} influx, and the current was sampled every second to resolve the time constant of the E_{rev} shifts better. The current at 10 mM BAPTA was fit best with two exponentials of 4.3 ± 0.5 and 70.2 ± 36.3 (χ^2 for two-exponential 0.4 ± 0.1 and for single exponential 3.0 ± 1.6). However, the Ca^{2+} current at 10 μM Ca^{2+} can be fit best with a single exponential time course, and thus Fig. 2 shows the time constants of the single exponential fits. Fig. 2 show that the time constant of the shift in E_{rev} is similar in the presence and absence of Ca^{2+} buffer and at a current density range of 80–550 pA/pF. If most of the shift in E_{rev} was because of Ca^{2+} accumulation, the time constant would have been strongly affected by current density and the Ca^{2+} buffer.

Additional evidence that part of the shift in the Ca^{2+} current E_{rev} is because of a change in channel pore properties is shown in supplemental Fig. S1: (i) TRPML3(A419P) retains part of

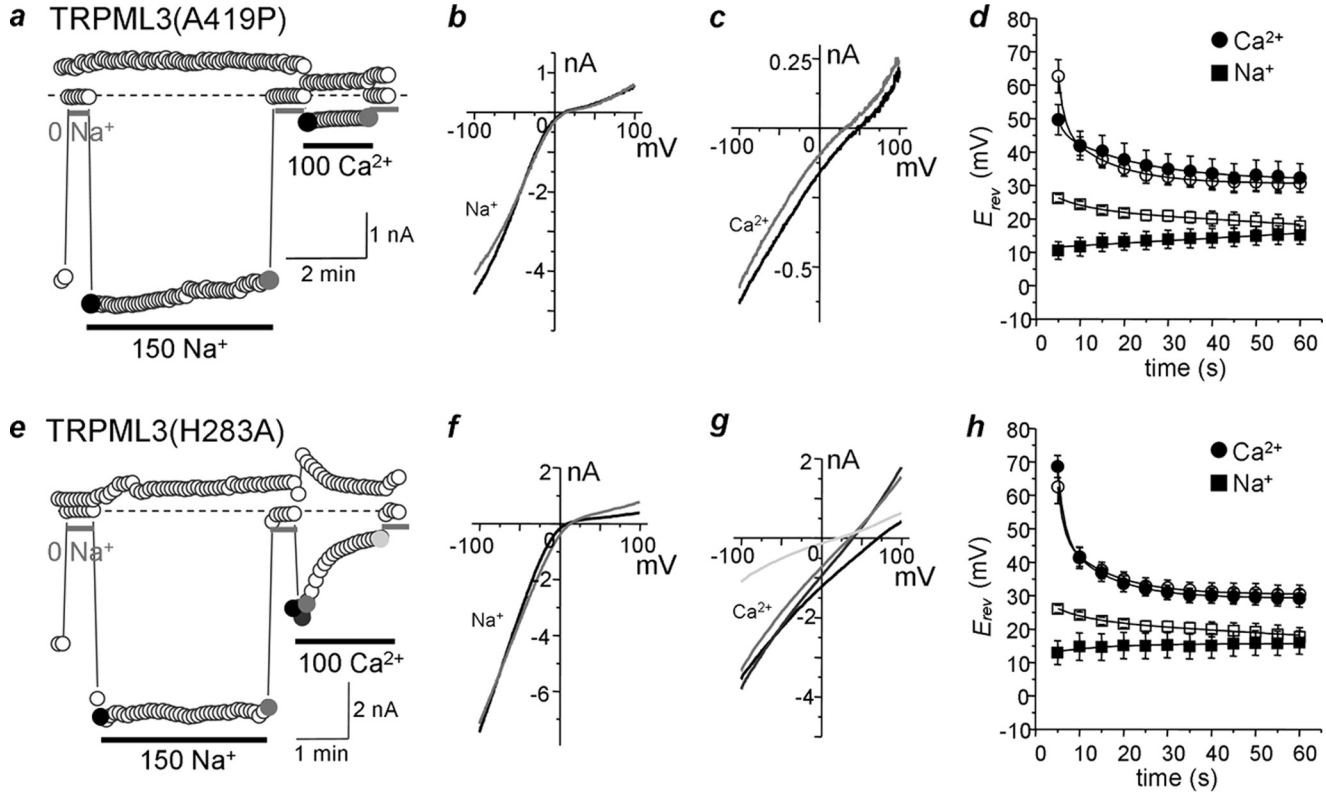

FIGURE 4. **Effect of the varitint-waddler phenotype causing A419P mutation on TRPML3 pore behavior.** *a* and *e*, whole cell currents of the A419P and H283A mutants were measured as in Fig. 1. *b* and *c*, *f* and *g*, *I/V* relationships for each mutant recorded at the times shown by the *large filled circles* in *a* and *e*. *d* and *h*, changes in E_{rev} for the first 1 min of current recording for each mutant. *Open symbols* are the E_{rev} for WT TRPML3. *Error bars*, S.E.

the E_{rev} shift (see below), whereas TRPML1(V432P), which shows similar inward rectifying Ca^{2+} current density as TRPML3(A419P), shows no E_{rev} shift (supplemental Fig. S1, *d–f*); (ii) TRPML3 mutants that reduce the Ca^{2+} conductance did not prolonged the time constant of the shift (supplemental Fig. S1*g*); (iii) Ca^{2+} current by the inward rectifying Orai1 had no obvious effect of the E_{rev} for Ca^{2+}. Although none of these criteria alone is sufficient, together they do indicate that the E_{rev} shift is at least in part due to a change in the TRPML3 pore properties for Ca^{2+}.

To examine the effect of the membrane potential on the shift in E_{rev}, we recorded the Ca^{2+} current while holding the membrane potential at +80 mV. Fig. 3*a* shows that the Ca^{2+} current develops normally at +80-mV holding potential, but the current does not undergo the fast inactivation observed at 0-mV holding potential (Fig. 1*a*). Fig. 3*b* shows that the shift in E_{rev} is prevented when the holding potential is +80 mV.

The effects of holding the membrane potential at +80 mV raise the possibility that the shift in E_{rev} and the fast inactivation of the Ca^{2+} current are mediated by Ca^{2+} binding to a site that regulates the pore. The positive membrane potential may prevent interaction of Ca^{2+} with or dislodge Ca^{2+} from this site. We tested this prediction first by repeated application of a solution containing 10 mM Ca^{2+}. Fig. 3*c* shows that after the initial fast inactivation, the channel remains partially inactivated on repeated application of 10 mM Ca^{2+}. Notably, Fig. 3*c* shows that E_{rev} remained shifted, even when the cells were incubated in Ca^{2+}-free solution containing 5 mM EGTA. Because of gradual channel inactivation we were able to alternately expose the channel to 10 mM Ca^{2+} and 5 mM EGTA up to four times and as long as 10 min. Yet, E_{rev} never recovered or showed significant farther shift. Fig. 3*d* shows that almost complete recovery of E_{rev} was obtained when TRPML3 was made to conduct Na^+ between Ca^{2+} current measurements, although the current magnitude did not recover. This suggests that Na^+ flow through the channel is necessary to displace Ca^{2+} from an inhibitory site in the pore.

It is possible that the shift in E_{rev} is mediated by Ca^{2+} binding to a deep pore site because removing intracellular Ca^{2+} with 10 BAPTA and extracellular Ca^{2+} by including 5 mM EGTA in the Na^+-free bath solution did not restore E_{rev} (Fig. 3*d*). This may be mediated by pore-lining charged residues that affect in the E_{rev} shift. A search for such potential residues is shown in supplemental Fig. S2*a*, which depicts the predicted lining of the negatively charged Glu^{449}, Asp^{458}, and Asp^{459} in the TRPML3 pore region. Glu^{449} is predicted to be in the pore helix, whereas Asp^{458} and Asp^{459} are predicted to line the selectivity filter. Mutation of Asp^{458} to lysine, alanine, or asparagine resulted in an inactive channel. The E449K mutation completely inhibited the channel. However, supplemental Fig. S2, *b–d* shows that the E449A mutation converted the channel to constitutively active, nearly eliminated inactivation of the Ca^{2+} current, and altered the shift in E_{rev}. The D459A mutation resulted in a marked decrease in Ca^{2+} permeability and selectivity and eliminated the shift in E_{rev} (supplemental Fig. S2, *e–g*). These findings suggest that Glu^{449} and Asp^{459} participate in the E_{rev} shift.

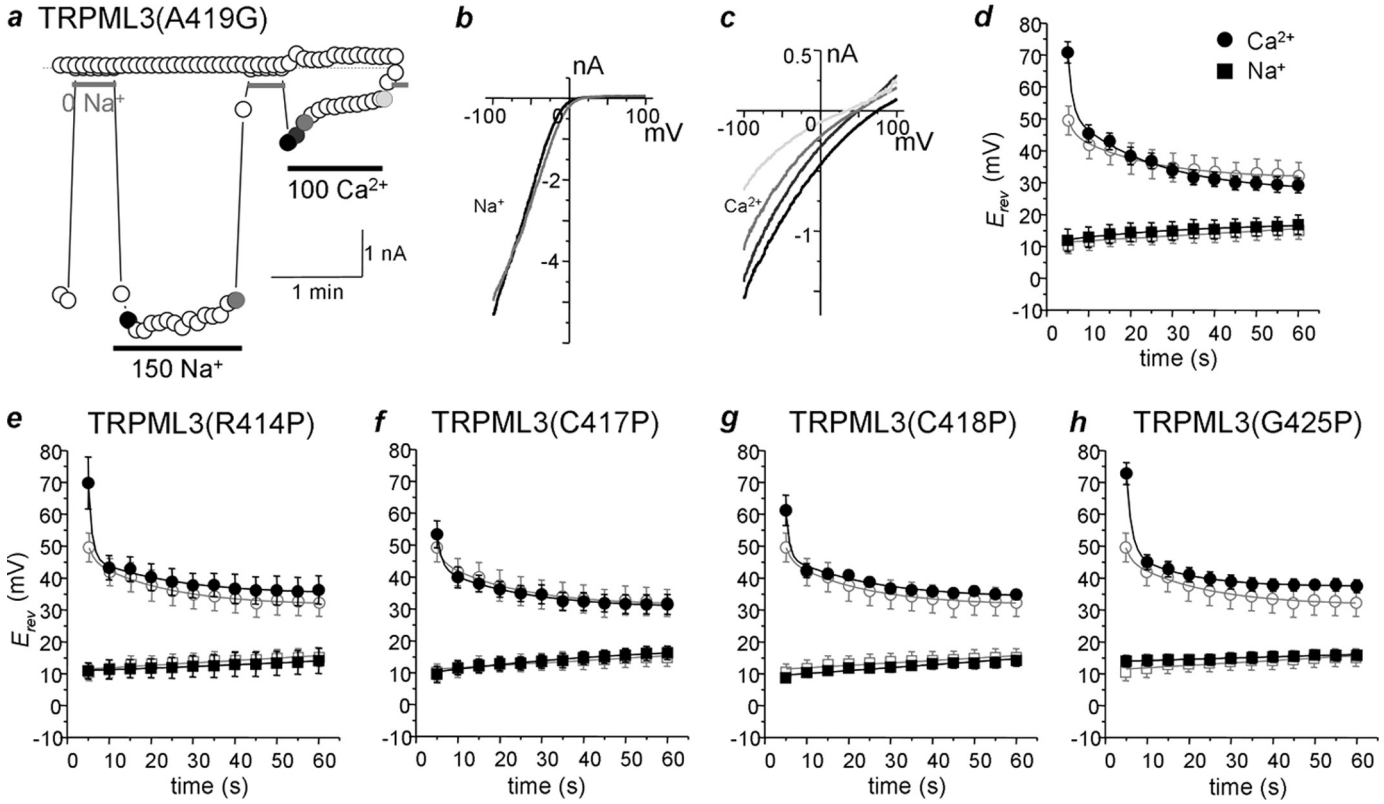

FIGURE 5. **Effect of fifth transmembrane domain mutations on the TRPML3 pore behavior.** *a*, whole cell current of the A419G mutant was measured as in Fig. 1. *b* and *c*, *I/V* relationships for TRPML3(A419G) recorded at the times shown by the *large filled circles* in *a*. *d–h*, E_{rev} changes for the first 1 min for each mutant. *Open symbols* are the E_{rev} changes for TRPML3(A419P). *Error bars*, S.E.

The results so far suggest that Ca^{2+} has two apparently independent effects on TRPML3. Ca^{2+} causes partial inhibition of the current and a shift in E_{rev} during Ca^{2+} conduction to reduce the pore selectivity for Ca^{2+}. The independence of the two effects is concluded from the restoration of E_{rev} for Ca^{2+} but not of the magnitude of either Ca^{2+} or Na^+ currents. On the other hand, the Na^+ current is fully restored on repeated alternate exposure of TRPML3 to Na^+-free and Na^+-containing media (6, 7). The shift in TRPML3 E_{rev} for Ca^{2+} is different from the shift in E_{rev} reported for TRPV1 (17, 18), TRPA1 (19, 20), and the P2X receptors (14, 16) in that it is not caused by agonist-mediated events, but is mediated by the conducted ion itself.

Effect of the Varitint-Waddler Phenotype-causing Mutation A419P on the Properties of the TRPML3 Pore—The A419P mutation locks TRPML3 in an open state and reduces its Ca^{2+} permeability (7), suggesting that it affects pore behavior. Hence, we characterized in detail the pore behavior of TRPML3(A419P). Fig. 4*a* confirms our previous finding (7) of constitutive activity of TRPML3(A419P) and low Ca^{2+}/Na^+ current ratio even at 100 mM Ca^{2+}. More important, Fig. 4, *b* and *c*, shows significantly reduced shift in E_{rev} when TRPML3(A419P) conducts Na^+ or Ca^{2+}. Fig. 4*d* and supplemental Table 1 show that the main effect of the A419P mutation is an increase in τ_2 to 21.48 ± 6.74 ($p = 0.03$). An additional effect of the A419P mutation is reduced selectivity for Ca^{2+}. The initial E_{rev} for Ca^{2+} of TRPML3 is 69.1 ± 4.6 mV whereas that for TRPML3(A419P) is 49.7 ± 4.5 mV (Fig. 4*d* and supplemental Table 2).

The findings with TRPML3(A419P) raised the question of whether the behavior of the TRPML3(A419P) pore is related to the GOF of this mutant. We addressed this question first by examining the pore properties of TRPML3(H283A) that have the same functional and cellular phenotype as TRPML3(A419P) (7). Fig. 4, *e–h*, shows that although TRPML3(H283A) shows reduced Ca^{2+} conductance (0.49 ± 0.08 Ca^{2+}/Na^+ current ratio), it retains the high Ca^{2+} selectivity, and the pattern of E_{rev} shift of the Ca^{2+} current is the same as that of TRPML3. Notably, although the Na^+ current by TRPML3(H283A) is spontaneously active and does not show time-dependent inactivation, TRPML3(H283A) retains the Ca^{2+}-dependent inactivation of the Ca^{2+} current. Hence, the altered properties of the TRPML3(A419P) pore are not simply related to the GOF.

Another proposed mechanism by which the A419P mutation can alter the TRPML3 pore is by disruption of the α-helical structure of the fifth TMD (7, 9, 13). This suggestion is based on the finding that mutation of Ala^{419} to glycine, another α-helix-disrupting residue, resulted in a GOF in TRPML3 (7, 9). We therefore analyzed the pore properties of TRPML3(A419G). Fig. 5*a* confirms the GOF of TRPML3(A419G) and shows that the A419G mutation reduced the Ca^{2+} conductance of the channel (0.27 ± 0.05 Ca^{2+}/Na^+ current ratio). Although the A419G mutation significantly changed τ_1 to 1.06 ± 0.12 and τ_2 to 21.77 ± 2.57 (supplemental Table 1), TRPML3(A419G) retains high Ca^{2+} selectivity and a large E_{rev} shift of the Ca^{2+} current (Fig. 5, *a–d*). Hence, the GOF and pore properties of

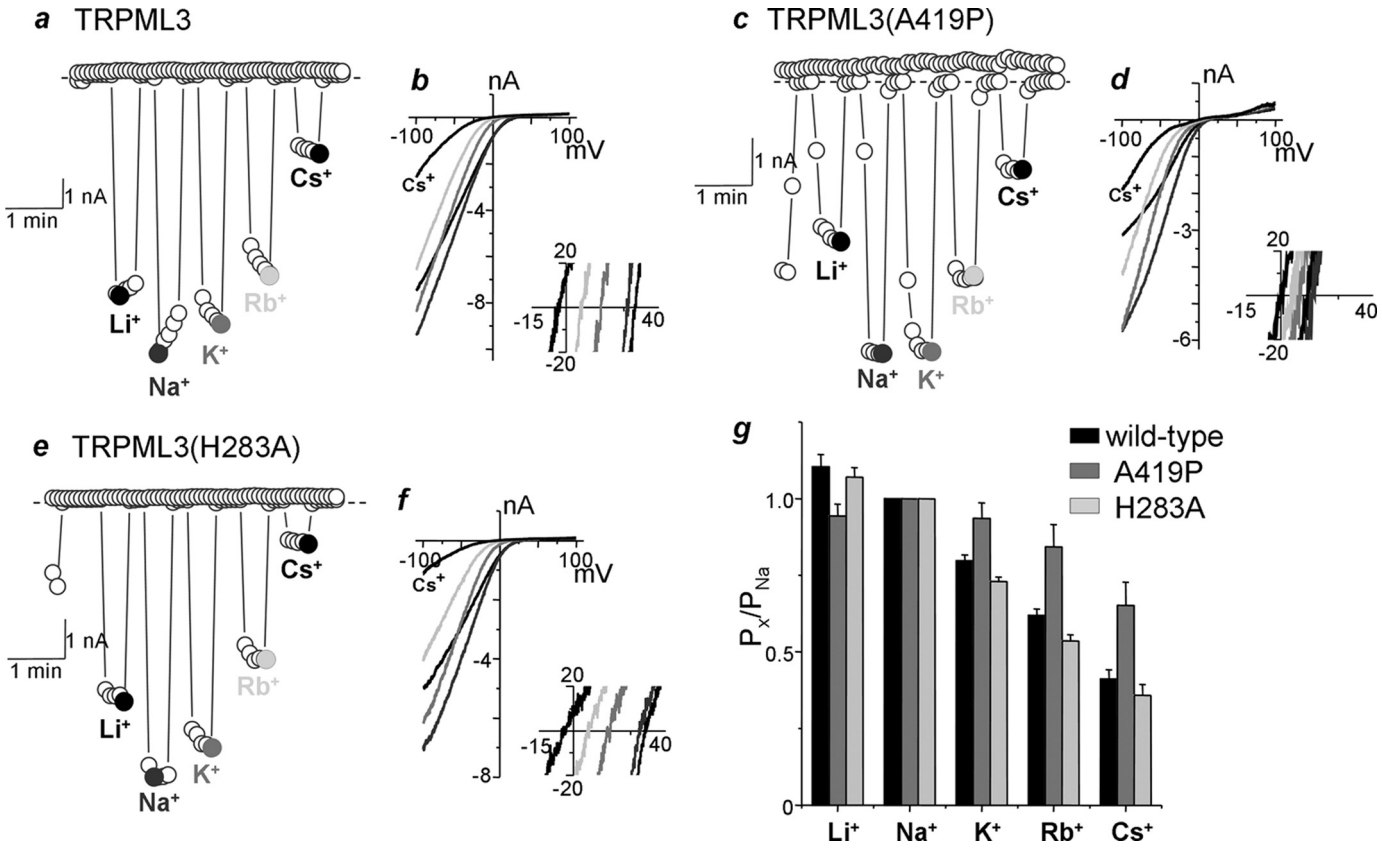

FIGURE 6. **Permeation profile of monovalent cations for WT and mutants TRPML3.** *a–f*, monovalent currents and *I/V* relationships were measured in extracellular solutions containing a 150 mM concentration of the indicated monovalent cation. Note the different permeability sequence for the TRPML3(A419P). *g*, summary of the relative permeability for WT and mutants TRPML3. The results are the mean ± S.E. (*error bars*) of 8–10 experiments.

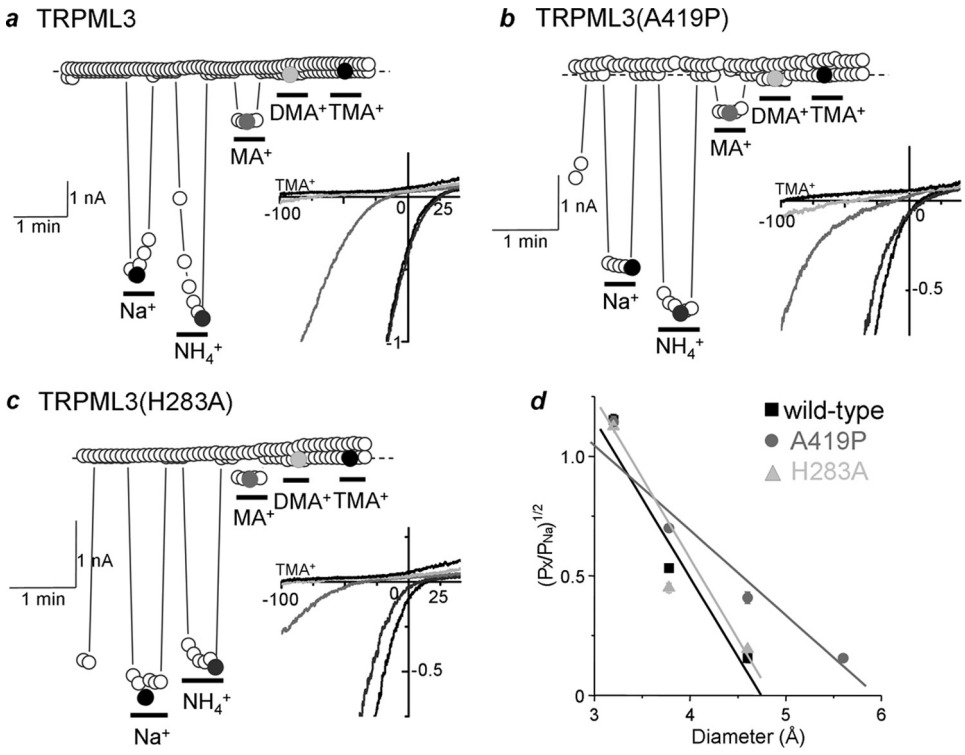

FIGURE 7. **Measurement of pore diameter.** *a–c*, HEK cells expressing the indicated TRPML3 constructs were exposed to extracellular solutions containing either 150 mM Na^+ or the indicated organic monovalent cations. *d*, permeability of the organic cations relative to Na^+ is plotted against the size of each cation ($n = 4–5$).

TRPML3(A419G) are similar to those of TRPML3(H283A), and the A419P mutation is not simply due to disruption of TRPML3 fifth TMD α-helical fold.

Because proline introduces kinks in α-helices and mutations of residues in the fifth TMD other than Ala^{419} to prolines result in GOF in TRPML3 (9), we tested the effect of mutating to proline residues N- and C-terminal to Ala^{419}. As reported previously (9), the R414P, C417P, C418P, and G425P mutations caused GOF in TRPML3. Fig. 5, *e–h*, and supplemental Tables 1 and 2 show that although all mutants are spontaneously active, the extents of their effect on pore properties are different. R414P and G425P had minimal effects, C418P had modest effect, and only C417P behaved similarly to the A419P mutant.

Together, the analysis in Figs. 4 and 5 suggests that the kink caused by A419P specifically alters properties of the TRPML3 pore. Below,

we characterize in greater details the effect of the A419P mutation on the TRPML3 pore.

A419P Mutation Affects TRPML3 Pore Field Ionic Strength—The results shown in Figs. 4 and 5 indicate that the A419P mutation directly affects the TRPML3 pore. To classify the pore properties of WT and mutants TRPML3, we determined the relative monovalent cation permeability of the channels. To measure the maximal current for each monovalent ion, the bath solution was alternately switched between Na^+-free solution and solutions containing a single permeant cation species to calculate the permeability and selectivity relative to Na^+. Fig. 6 shows that for TRPML3, the permeability ratios for Li^+, K^+, Rb^+, and Cs^+ relative to Na^+ were 1.10 ± 0.04, 0.80 ± 0.02, 0.62 ± 0.02, and 0.41 ± 0.03, respectively. This sequence ($Li^+ > Na^+ > K^+ > Rb^+ > Cs^+$) corresponds to Eisenman sequence XI, indicating a strong field strength site. The GOF mutation H283A has the same permeability sequence and thus does not change the pore architecture. By contrast, TRPML3(A419P) poorly discriminates between monovalent cations and resulted in the selectivity sequence of $Na^+ > Li^+ > K^+ > Rb^+ > Cs^+$, which corresponds to Eisenman sequence X. These results are consistent with the conclusion that the A419P mutation causes a conformational change in the TRPML3 pore to change its architecture.

A419P Mutation Increases the Diameter of the TRPML3 Pore—The change in pore selectivity of TRPML3(A419P) to a weaker field strength can reflect an increased pore size. To test this possibility, we estimated the pore diameter of WT and mutants TRPML3 by measuring their relative permeability to organic monovalent cations of increasing size (19, 21, 22). We tested the permeability of ions with the following sizes (23): ammonium (A^+), 3.2 Å; methylammonium (MA^+), 3.78 Å; dimethylammonium (DMA^+), 4.6 Å; and tetramethylammonium (TMA^+), 5.6 Å. Fig. 7, *a–c*, show that TRPML3 and TRPML3(H283A) conducted a small current with MA^+ but failed to conduct DMA^+ and TMA^+. By contrast, DMA^+ current was measurable with the A419P mutant. The pore diameter of the channels was estimated using the excluded volume equation (17, 19, 21, 24). Estimates of pore diameter for TRPML3, TRPML3(H283A), and TRPML3(A419P) are 4.73, 4.82, and 5.94 Å, respectively (Fig. 7*d*). These results suggest that the GOF of TRPML3(A419P) results from about 30% stable expansion of the channel pore.

CONCLUSIONS

The present findings reveal a unique form of pore behavior of the TRPML3 Ca^{2+} channel. Measurement of Ca^{2+} current shows that the current undergoes a rapid shift in E_{rev} to result in altered pore properties. This process is regulated by Ca^{2+} that interacts with a pore site that does not have readily access to cytosolic or extracytosolic face of the channel. The pore lining-charged residues Glu^{449} and Asp^{459} appear to participate in the potential binding site for the regulatory Ca^{2+}. Modeling suggests that in the tetramer these residues form two adjacent rings of negative charges next to the cytoplasmic channel vestibule. Ca^{2+} binding to this site reduces the selectivity and permeability of the channel for Ca^{2+}. This may serve as a protective mechanism to limit Ca^{2+} flux by the channel. Maintained activity of TRPML3 is highly toxic, as evident from the varitint-waddler phenotype (4) and from cell death that occurs by expression of TRPML3(A419P) (6, 8–10, 25) and the TRPML3(H283A) (7) GOF mutations in model systems. The toxicity is caused by excessive Ca^{2+} influx (6–10, 25). Hence, the reduction in selectivity and permeability of TRPML3 by Ca^{2+} allows limited Ca^{2+} flow through the active channel by rapidly reducing the flow and by increasing the conduction of monovalent ions relative to Ca^{2+}.

Change in TRP channel selectivity as described here for TRPML3 may be a more general mechanism for regulation of Ca^{2+} flow by the TRP channels. Many TRP channels are regulated by Ca^{2+} (1, 2), and negative charges are present in the predicted pores of many TRP channels (1). It is thus possible that these negatively charged residues have a function similar to Glu^{449} and Asp^{459} found here for TRPML3. This possibility is supported by recent findings showing that Asp^{646} in TRPV1 (17) and Asp^{918} in TRPA1 (19) participate in the alteration of E_{rev} observed after activation of the channels by ligands.

Acknowledgment—We thank Dr. Michael Dorwart for help with the modeling.

REFERENCES

1. Nilius, B., Owsianik, G., Voets, T., and Peters, J. A. (2007) *Physiol. Rev.* **87,** 165–217
2. Venkatachalam, K., and Montell, C. (2007) *Annu. Rev. Biochem.* **76,** 387–417
3. Bargal, R., Avidan, N., Ben-Asher, E., Olender, Z., Zeigler, M., Frumkin, A., Raas-Rothschild, A., Glusman, G., Lancet, D., and Bach, G. (2000) *Nat. Genet.* **26,** 118–123
4. Atiba-Davies, M., and Noben-Trauth, K. (2007) *Biochim. Biophys. Acta* **1772,** 1028–1031
5. Di Palma, F., Belyantseva, I. A., Kim, H. J., Vogt, T. F., Kachar, B., and Noben-Trauth, K. (2002) *Proc. Natl. Acad. Sci. U.S.A.* **99,** 14994-14999
6. Kim, H. J., Li, Q., Tjon-Kon-Sang, S., So, I., Kiselyov, K., and Muallem, S. (2007) *J. Biol. Chem.* **282,** 36138–36142
7. Kim, H. J., Li, Q., Tjon-Kon-Sang, S., So, I., Kiselyov, K., Soyombo, A. A., and Muallem, S. (2008) *EMBO J.* **27,** 1197–1205
8. Nagata, K., Zheng, L., Madathany, T., Castiglioni, A. J., Bartles, J. R., and García-Añoveros, J. (2008) *Proc. Natl. Acad. Sci. U.S.A.* **105,** 353–358
9. Grimm, C., Cuajungco, M. P., van Aken, A. F., Schnee, M., Jörs, S., Kros, C. J., Ricci, A. J., and Heller, S. (2007) *Proc. Natl. Acad. Sci. U.S.A.* **104,** 19583–19588
10. Xu, H., Delling, M., Li, L., Dong, X., and Clapham, D. E. (2007) *Proc. Natl. Acad. Sci. U.S.A.* **104,** 18321–18326
11. Kim, H. J., Soyombo, A. A., Tjon-Kon-Sang, S., So, I., and Muallem, S. (2009) *Traffic* **10,** 1157–1167
12. Martina, J. A., Lelouvier, B., and Puertollano, R. (2009) *Traffic* **10,** 1143–1156
13. Cuajungco, M. P., and Samie, M. A. (2008) *Pflügers Arch.* **457,** 463–473
14. Khakh, B. S., and North, R. A. (2006) *Nature* **442,** 527–532
15. Virginio, C., MacKenzie, A., Rassendren, F. A., North, R. A., and Surprenant, A. (1999) *Nat. Neurosci.* **2,** 315–321
16. North, R. A. (2002) *Physiol. Rev.* **82,** 1013–1067
17. Chung, M. K., Güler, A. D., and Caterina, M. J. (2008) *Nat. Neurosci.* **11,** 555–564
18. Samways, D. S., Khakh, B. S., and Egan, T. M. (2008) *J. Biol. Chem.* **283,** 31274–31278
19. Karashima, Y., Prenen, J., Talavera, K., Janssens, A., Voets, T., and Nilius,

B. (2010) *Biophys. J.* **98,** 773–783
20. Chen, J., Kim, D., Bianchi, B. R., Cavanaugh, E. J., Faltynek, C. R., Kym, P. R., and Reilly, R. M. (2009) *Mol. Pain* **5,** 3
21. Sabovcik, R., Li, J., Kucera, P., and Prod'hom, B. (1995) *J. Gen. Physiol.* **106,** 149–174
22. Voets, T., Janssens, A., Droogmans, G., and Nilius, B. (2004) *J. Biol. Chem.* **279,** 15223–15230
23. Liu, D. M., and Adams, D. J. (2001) *J. Physiol.* **534,** 423–435
24. Dwyer, T. M., Adams, D. J., and Hille, B. (1980) *J. Gen. Physiol.* **75,** 469–492
25. Lev, S., Zeevi, D. A., Frumkin, A., Offen-Glasner, V., Bach, G., and Minke, B. (2010) *J. Biol. Chem.* **285,** 2771–2782